JOURNAL OF COMPUTATIONAL PHYSICS 82, 16–28 (1989)

Complex Prüfer Phase Function with Applications to Scattering

PETRI PAJUNEN

Department of Chemistry, University of Oulu, Linnanmaa, SF-90570 Oulu 57, Finland

Received September 10, 1987; revised June 13, 1988

The Prüfer phase function method is extended to full complex formalism whereby parameters, functions, and integration paths may all be complex-valued. A procedure for tracing the relevant integration paths is presented. We use as illustrations, applications to scattering theory: calculation of complex optical phase shifts, evaluation of quantal deflection function, and location of quantal rainbows are presented. © 1989 Academic Press, Inc.

1. INTRODUCTION

The Prüfer phase function provides a powerful computational tool for many problems in applied mathematics, physics, chemistry, and engineering typically arising from phenomena described by waves such as electromagnetic radiation, fluid waves, or quantum mechanical wave phenomenon. The most common application of the Prüfer phase function is the Sturm–Liouville eigenvalue problem: finding the eigenvalue λ_1, say, that yields a non-zero solution $\Psi(x)$ of a differential equation of the form

$$\Psi''(x) + Q(x; \{\lambda_j\})\, \Psi(x) = 0, \tag{1}$$

where $\{\lambda_j\}$ denotes parameters of the function $Q(x)$, subject to suitable boundary conditions at the endpoints of the relevant interval on the real line. The present article deals with several extensions of this basic case, the most fundamental of which is the full complex formalism: the parameters, all the functions, and the integration paths of Eq. (1) are allowed to be complex. Illustrated by example applications, several different types of computational problems are considered such as complex quantization, a problem for which the desired quantity is not an eigenparameter but is obtained from the value of the Prüfer phase function at a certain point or interval in the complex plane and a case in which the desired quantity is a function derived from the Prüfer phase function by explicit differentiation. While the former of these applications only deal with a straightforward integration of a differential equation for the appropriate phase function, such as

$$\theta'(z; \{\lambda_j\}) = -\sin^2 \theta(z; \{\lambda_j\}) - Q(z; \{\lambda_j\}) \cos^2 \theta(z; \{\lambda_j\}) \tag{2}$$

0021-9991/89 $3.00

in the case of the unmodified Prüfer phase function, the last case also involves additional differential equations for a function obtained by explicit differentiation of an equation similar to Eq. (2).

The complex integration method and applications similar to those considered in the present article are likely to appear in many problems in the fields mentioned above. However, to illustrate the procedure, specific applications to potential scattering are considered. In the following, Section 2 presents the two Prüfer phase functions considered in this work, their relation and their respective differential equations and a general procedure for generating new relevant functions and their differential equations. Section 3 then deals with the complex integration and provides means of tracing the integration paths in the complex plane. Sections 4, 5, and 6 present specific applications: calculations of complex quantal scattering phase shifts and quantal deflection function, and location of quantal rainbows and saddles directly from the Prüfer phase function method or by a complex quantization calculation. Numerical results are collected in Section 7 and conclusions are finally summed up in Section 8.

2. The Prüfer Phase Functions

The usual Prüfer phase function method [1–5] for solving Eq. (1) utilizes the logarithmic derivative of $\Psi(z)$ in the form of the Prüfer substitution

$$\frac{\Psi'(z)}{\Psi(z)} = \tan \theta(z; \{\lambda_j\}) \tag{3}$$

or the modified Prüfer substitution

$$\frac{\Psi'(z)}{\Psi(z)} = Q^{1/2}(z; \{\lambda_j\}) \tan \varphi(z; \{\lambda_j\}) \tag{4}$$

to transform the second-order differential equation, Eq. (1), to two first-order equations, one of which, involving $\theta(z; \{\lambda_j\})$ or $\varphi(z; \{\lambda_j\})$, is independent of the solution of the other equation. For the present calculations, however, slightly more general functions are more appropriate. Therefore, in order to have a direct relation between the asymptotic values of the phase functions $\theta(z; \{\lambda_j\})$ or $\varphi(z; \{\lambda_j\})$ and the physical quantities considered in later applications, substitutions

$$\frac{\Psi'(z)}{\Psi(z)} = \tan(\theta(z; \{\lambda_j\}) + kz) \tag{5}$$

and

$$\frac{\Psi'(z)}{\Psi(z)} = Q^{1/2}(z; \{\lambda_j\}) \tan(\varphi(z; \{\lambda_j\}) + kz), \tag{6}$$

where k is a constant depending on the problem, were used in the present work yielding for $\theta(z; \{\lambda_j\})$ or $\varphi(z; \{\lambda_j\})$ the first-order differential equations

$$\theta'(z; \{\lambda_j\}) = -k - Q(z; \{\lambda_j\}) \cos^2(\theta(z; \{\lambda_j\}) + kz) - \sin^2(\theta(z; \{\lambda_j\}) + kz) \quad (7)$$

and

$$\varphi'(z; \{\lambda_j\}) = -k - Q^{1/2}(z; \{\lambda_j\}) - \frac{Q'(z; \{\lambda_j\})}{4Q(z; \{\lambda_j\})} \sin(2(\varphi(z; \{\lambda_j\}) + kz)). \quad (8)$$

The choice between Eqs. (7) and (8) is based on computational convenience bearing in mind that the relation

$$\tan(\theta(z; \{\lambda_j\}) + kz) = Q^{1/2}(z; \{\lambda_j\}) \tan(\varphi(z; \{\lambda_j\}) + kz) \quad (9)$$

can be used to change from one representation to the other provided $Q(z; \{\lambda_j\}) \neq 0$. The computations using Eqs. (7) and (8) are subjected to the following numerical restrictions. The φ-representation cannot be used in the immediate neighbourhood of a zero of $Q(z; \{\lambda_j\})$, called a turning point. On the other hand, if $Q(z; \{\lambda_j\})$ is large (and positive) the φ-integration is more stable and numerically the more accurate of the two representations while the θ-equation for such circumstances suffers from truncation errors. Therefore, if integration through a turning point is required, a typical procedure would be to start the integration with the θ-equation, integrate past the contributing turning points, and then change to φ-representation via Eq. (9).

While in many problems the required quantity may be immediately computed from the value of one of the phase functions above, for some other problems the desired quantities are functions of various partial derivatives of a phase function with respect to the parameters $\{\lambda_j\}$. A fairly complicated system of this kind is presented in [6] but, for simplicity, the present work only considers a case involving a simple partial derivative with respect to one of the parameters, λ_i. A straightforward differentiation of Eq. (8) immediately yields the differential equation for

$$\begin{aligned}\zeta'(z; \{\lambda_j\}) \equiv \left(\frac{\partial \varphi'(z; \{\lambda_j\})}{\partial \lambda_i}\right) &= -\frac{1}{2}\left(\frac{\partial Q(z; \{\lambda_j\})}{\partial \lambda_i}\right) Q^{-1/2}(z; \{\lambda_j\}) \\ &\quad -\frac{1}{4}\left(\frac{\partial Q'(z; \{\lambda_j\})/\partial \lambda_i}{Q(z; \{\lambda_j\})} - \frac{Q'(z; \{\lambda_j\})\, \partial Q(z; \{\lambda_j\})/\partial \lambda_i}{Q^2(z; \{\lambda_j\})}\right) \\ &\quad \times \sin(2(\varphi(z; \{\lambda_j\}) + kz)) \\ &\quad -\frac{Q'(z; \{\lambda_j\})}{2Q(z; \{\lambda_j\})} \cos(2(\varphi(z; \{\lambda_j\}) + kz)) \left(\zeta(z; \{\lambda_j\}) + z\frac{\partial k}{\partial \lambda_i}\right) \quad (10)\end{aligned}$$

which can be integrated with Eq. (8) along the integration paths described below subject to relevant boundary conditions depending on the particular problem.

3. Integration Paths in the Complex Plane

For real problems the integration takes place along the real line and the only computational difficulties are associated with the turning points as discussed above. The codes available by now [7, 8] cope with this by employing the unmodified, Eq. (2), or the so-called scaled Prüfer substitution which essentially amounts to imitating $Q(z; \{\lambda_j\})$ in Eq. (4) by local approximations except near the turning points to avoid the difficulties associated with the zeros of $Q(z; \{\lambda_j\})$. For the problems considered in this work, it is clearly desirable to use only one representation, θ- or φ-one, because while Eq. (9) is very straightforward to use, similar equations for the ζ-function and similar, even more complicated, functions would be prohibitively unwieldy.

For the complex case, as explained in [9], the role of the real axis as the integration path is taken by a path in the complex z-plane consisting of Stokes' lines and anti-Stokes' lines emerging from the complex turning points contributing to the problem. These lines are defined as paths in the complex z-plane on which $Q^{1/2}\,dz$ is purely imaginary or purely real, respectively. As a particular case, in the real problem, for which dz is dx and Q real negative or positive, the classically forbidden regions "outside" the turning points, where Q is negative and thus $Q^{1/2}$ imaginary, are Stokes' lines and the classically allowed regions where Q is positive are anti-Stokes' lines. For a general problem, a straightforward application of the conditions above shows that the lines are defined by the differential equations

$$\frac{dy}{dx} = -\frac{\mathrm{Re}(Q^{1/2})}{\mathrm{Im}(Q^{1/2})}, \qquad \text{for a Stokes' line,} \tag{11}$$

$$\frac{dy}{dx} = \frac{\mathrm{Im}(Q^{1/2})}{\mathrm{Re}(Q^{1/2})}, \qquad \text{for an anti-Stokes' line,} \tag{12}$$

where $z = x + iy$ and $Q^{1/2} = \mathrm{Re}(Q^{1/2}) + i\,\mathrm{Im}(Q^{1/2})$. For accurate results, the integration must approximately follow the path defined by the relevant Stokes' lines and anti-Stokes' lines of the problem with special attention to the Stokes' lines. On a Stokes' line, Eq. (1) has exponentially increasing and decreasing solutions and the integration obviously soon picks up the exponentially increasing solution. Therefore, on a Stokes' line, the integration is carried out towards the turning point to ensure an accurate transition to the oscillatory solution on an anti-Stokes' line. On an anti-Stokes' line on the other hand, the direction of the integration is not crucial. Figures 1a–d show some typical distributions of turning points and associated appropriate paths. Figure 1a presents the integration path for a straightforward one-turning-point calculation of real or complex phase shift with one Stokes' line and one anti-Stokes' line while Fig. 1b shows a real three-turning-point near-resonance case in which, for calculation of the phase shift, the Stokes' line at the left must be connected to the anti-Stokes' line emerging from the rightmost turning point. Figure 1c depicts a similar complex case in which the integration path essentially is reduced to the case of Fig. 1a because the two turning points on the right

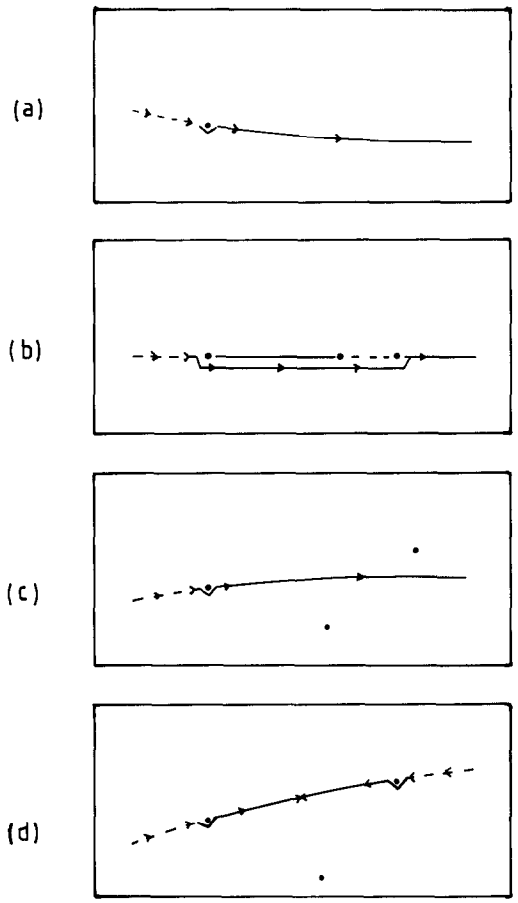

FIG. 1. Typical turning point distributions, Stokes' lines (broken), anti-Stokes' lines (full) and appropriate integration paths (arrows) for (a) one-turning-point phase shift calculation; (b) real three-turning-points near-resonance phase shift calculation; (c) near-resonance phase shift calculation with extra turning points; (d) complex angular momentum resonance situation.

only affect the numerical efficiency of the calculation, in particular with phase-integral methods. Finally, Fig. 1d shows complex angular momentum resonance situation. In this case, the two relevant turning points correspond to the leftmost and rightmost turning points of Fig. 1b while the third turning point has moved down and is not significant. The integration path and the behaviour of the system are very similar to familiar bound states.

While the complications at the turning points prevent the real codes of using the modified Prüfer transformation, Eq. (4), the complex formalism of the present work does not suffer from this restriction because the path can be transformed to form a small circle or a kink to avoid the immediate neighbourhood of the turning point. The codes of the present work therefore always use the φ-equations in integrations

and follow the integration path traced out by pathfinders based on the differential equations (11) and (12) which, with the initial input of the location of the relevant turning point, routinely yield the curves in terms of arrays of x, y-values using the Runge–Kutta–Merson method of the routine D02BBF of the NAG library. The turning points are avoided by making a small kink in the complex plane. The θ-representation is occasionally used to input appropriate boundary conditions with the aid of Eq. (9).

The exact numerical integration above can be used to obtain results of virtually any desired accuracy. However, for most situations, as shown in [5], the best compromise between high accuracy and cost of computation is to use high-order phase integral quadrature to integrate the phase function. For the scattering applications below, as a rule of thumb, it has been found out that if the number of contributing turning points is one, the high-order phase integral method yields the best possible compromise between high accuracy and computational efficiency, but if the number of relevant turning points is more than one, the increased complexity of the phase integral formulae combined with possible computational complications favor the direct numerical integration of the phase functions.

4. The Prüfer Phase Function Phase Shift Calculation

The traditional definition of the phase shift δ_l follows from the boundary conditions of the radial Schrödinger equation

$$\Psi_l''(r)+\left[k^2-\frac{2\mu}{\hbar^2}V(r)-\frac{l(l+1)}{r^2}\right]\Psi(r)=0, \tag{13}$$

where $l=0, 1, 2, 3, \ldots$ is the orbital angular momentum number, at $r=0$,

$$\Psi_l(0)=0, \tag{14}$$

and, at infinity,

$$\Psi_l(r)\underset{r\to\infty}{\simeq}\sin\left(kr-\frac{l\pi}{2}+\delta_l\right). \tag{15}$$

The definition above, which implies integration along the real line, is strictly valid for real phase shifts only. For complex phase shifts, the turning point responsible for the phase shift lies in the complex plane off the real axis. Accordingly, as explained above, the role of the real axis is taken by a complex path consisting of a Stokes' line and an anti-Stokes' line emerging from this complex turning point.

The notation

$$Q(z)=\left[k^2-\frac{2\mu}{\hbar^2}V(r)-\frac{l(l+1)}{r^2}\right] \tag{16}$$

brings Eq. (13) in line with Sections 2 and 3 and from Eqs. (6) and (15) it follows that, apart from a constant factor $\pi/2$, $\varphi(z)$ corresponds to the argument of the sin-function of Eq. (15). Therefore, according to the boundary conditions corresponding Eqs. (14) and (15), the complex phase shift is obtained by integrating Eq. (8) from z small to z large along the complex integration path subject to the boundary condition $\theta(z) = -\pi/2$ at the starting point, from the relation

$$\delta_l = \varphi(z \to \infty) + l\pi/2. \tag{17}$$

The failure to follow the appropriate integration path such as integration along the real line in the complex case causes loss of accuracy and the appearance of unphysical multiples of π in the real part of the phase shift [10]. The phase integral evaluation of the phase shift in the complex case [11] implicitly chooses the correct integration path and is applicable with limitations described in [12, 13] and above.

5. The Prüfer Phase Function Quantum Deflection Function

Classical deflection function which is of great value in interpreting the features of the differential cross section is usually related to quantal scattering phase shift via the semiclassical phase shift expression [14, 15]. This method, however, introduces unnecessary complications due to the phase integral approximation and has a severely restricted range of validity. In particular, it is not applicable for energies near the orbiting resonances. The quantum deflection function is defined in terms of the partial derivative of the phase shift with respect to the angular momentum l

$$\Theta(l) = 2\frac{\partial\delta(l)}{\partial l} \tag{18}$$

and may thus be computed by numerical differentiation of the phase shift function. By substituting $Q(z)$ from Eq. (16) and by identifying λ_i with l in Eq. (10) the Prüfer phase function method immediately yields an explicit differential equation for

$$\begin{aligned}\left(\frac{\partial\varphi'(z)}{\partial l}\right) = {} & \frac{1}{2}\frac{(2(l+1))}{r^2}Q^{-1/2}(z) \\ & -\frac{1}{4}\left(\frac{2(2l+1)}{r^3Q(z)} + \frac{(2l+1)\,Q'(z)}{r^2Q^2(z)}\right)\sin(2(\varphi(z)+kz)) \\ & -\frac{Q'(z)}{2Q(z)}\cos(2(\varphi(z)+kz))\left(\frac{\partial\varphi(z)}{\partial l}\right)\end{aligned} \tag{19}$$

from which the quantum deflection function can be computed directly by integration subject to boundary conditions derived from Eqs. (14) and (15) and noting

that the solution of Eq. (19) requires a simultaneous integration of Eq. (8) to supply the values of the φ-function. A further differentiation of Eq. (19) yields yet another similar equation for

$$\frac{\partial \Theta(l)}{\partial l} = 2 \frac{\partial^2 \delta(l)}{\partial l^2} \tag{20}$$

so that the location of rainbows defined as the value of l for which the real deflection function has a minimum is reduced to the simple computational task of finding the value of l for which the function $\partial \Theta(l)/\partial l$ has a zero. Similarly, saddles which are complex are defined as the complex value of l for which the deflection function equals to the complex scattering angle.

6. Complex Angular Momentum Parametrization

The application of complex angular momentum techniques [16] to the problem of locating the rainbows and saddles associates the real and the imaginary parts of the value of the complex angular momentum at the pole with the position and the width of the deflection function minimum, respectively. Recalling that

$$S_l(k) = \exp 2i\delta_l, \tag{21}$$

where $S_l(k)$ is the diagonal S-matrix element, and parametrizing

$$S_l(k) = \frac{l - l_p^*}{l - l_p}, \tag{22}$$

it follows that the deflection function has a minimum at

$$l = \operatorname{Re} l_p \tag{23}$$

with a width given by

$$\Gamma_{df} = 2 \operatorname{Im} l_p, \tag{24}$$

where l_p is the complex angular momentum pole location which is evaluated by a straightforward complex eigenvalue calculation.

Remler [17], by using the first-order JWKB method, has parametrized the S-matrix element $S_l(k)$ in the semiclassical tradition by using the variable $l + \frac{1}{2}$. However, in a more accurate quantal calculation such as the present one, the parametrization of Eq. (22) is more natural. This simple parametrization is a useful computational device but has a somewhat restricted range of validity. The real part can be compared directly with the value from the direct method of Section 5 and

the width of the direct method is associated with the value of the deflection function at the minimum by

$$\Gamma_{df} = \frac{2}{\Theta^{\min}}. \tag{25}$$

7. Numerical Results

The computational methods described above were tested by calculating phase shifts and deflection functions for a wide range of l and locating deflection function minima for an analytic test potential

$$V(z) = 4\varepsilon\left[\left(\frac{\sigma}{r}\right)^{12} - \left(\frac{\sigma}{r}\right)^{6} - iW\left(\frac{\sigma}{r}\right)^{s}\right], \tag{26}$$

with $B = 2\mu\varepsilon\sigma^2/\hbar^2 = 125$. The reduced energy $K = A^2/B$, where $A = k\sigma$, and $C = 2\mu W\sigma^2/\hbar^2$ is the measure of the strength of the imaginary part of the potential relative to its real part.

Tables I and II present results for the real potential $C = 0$ for a range of the reduced energy including the low energy, multiple-turning-points, orbiting resonance region. Table I lists values of the phase shifts at $K = 0.2$ and $K = 0.5$ for a range of the partial wave index l in the resonance region and in Table II, locations of the rainbows and the values of the deflection function at the rainbow are given for a wide range of the reduced energy including those of Table I. The codes of the present work have a facility of the phase integral calculation of phase shifts which if applicable is computationally the most economical method of computing accurate phase shifts [5, 11]. However, as discussed in [13], the presence of an orbiting resonance may cause numerical difficulties which induce serious errors for the phase integral phase shifts for the few values of the partial wave index l near the resonance. This is very unfortunate because the main purpose of computing phase shifts is to evaluate the partial wave sum for cross section calculation and even a single inaccurate phase shift can seriously disturb the whole calculation. The present method therefore provides a remedy to the difficulties such as reported in [13] combining the computationally efficient phase integral quadrature and the exact numerical integration of the phase function to one accurate and efficient code.

The standard procedure for computing the deflection function is by phase integral methods and difficulties with multiple turning points have so far prevented calculations at the resonance region. Table II lists the positions and widths of the rainbows defined as the minima of the deflection function as well as the values of the deflection function at those points computed by the methods described above for a wide range of energies. From the comparisons of Table II it can be seen that, for energies below the top of the centrifugal barrier, $K \leqslant 0.5$, for the present poten-

TABLE I

Two Values of Reduced Energy K below the Top of the Barrier, Prüfer Phase Function Phase Shifts δ_l

	$K = 0.2$	$K = 0.5$
l	δ_l	δ_l
0	-0.48303	-4.26023
1	0.92825	-2.80291
2	2.17805	-1.45983
3	3.26233	-0.23252
4	4.17450	0.87659
5	4.90478	1.86407
6	5.43920	2.72524
7	5.75775	3.45384
8	5.82575	4.04146
9	5.52616	4.47655
10	4.55645	4.74246
11	3.78849	4.81381
12	0.40576	4.65522
13	0.23496	4.24753
14	0.15685	3.41257
15	0.10947	1.02973
16	0.07880	0.59601
17	0.05810	0.40755
18	0.04368	0.29471

Note. For LJ(12, 6) potential with $B = 125$.

tial, calculations with the computationally more efficient complex angular momentum parametrization are sufficiently accurate but for higher energies the parametrization of Eq. (22) becomes less valid and the direct method has to be used.

The complex integration procedure was tested by computing phase shifts for $C = 125$, $s = 10$ at a wide range of l for $K = 0.648$, $K = 2.592$, and $K = 10.368$. While

TABLE II

Positions and Widths of the Rainbows

	(a)		(b)		(c)
K	*Rel*	*Iml*	*Rel*	*Iml*	Θ^{min}
0.1			10.9605	0.00004	-53000.
0.2			11.8583	0.0057	-350.
0.3			12.2413	0.0493	-40.5
0.4	13.5804	0.1387	13.5809	0.1449	-14.424
0.5	14.3594	0.2525	14.3606	0.2741	-7.9210
0.6	15.0814	0.3738	15.0842	0.4184	-5.3508
0.7	15.7545	0.4959	15.7592	0.5686	-4.0332
0.8	16.3868	0.6165	16.3928	0.7200	-3.2439
0.9	16.9848	0.7351	16.9910	0.8700	-2.7206
1.0	17.5541	0.8517	17.5587	1.0174	-2.3483
1.2	18.6215	1.0792			-1.8532
1.4	19.6137	1.3007			-1.5374
1.6	20.5462	1.5182			-1.3173
1.8	21.4296	1.7322			-1.1546
2.0	22.2721	1.9436			-1.0290
2.5	24.3212	2.4639			-0.8117
3.0	26.0241	2.9764			-0.6719
3.5	27.6891	3.4839			-0.5741
4.0	29.2767	3.9878			-0.5015
4.5	30.7622	4.4892			-0.4455
5.0	32.1744	4.9887			-0.4092

Note. For LJ(12, 6) potential with $B = 125$, at the reduced energy range $K = 0.1$–5.0: (a) the Prüfer phase function method, (b) complex angular momentum method, and (c) the value of the quantum deflection function at the rainbow.

TABLE III

Complex Prüfer Phase Function Phase Shifts δ_l

	$K = 0.648$		$K = 2.592$		$K = 10.368$	
l	$Re\delta_l$	$Im\delta_l$	$Re\delta_l$	$Im\delta_l$	$Re\delta_l$	$Im\delta_l$
0	-5.658026	0.871824	-15.103387	0.872865	-31.098687	0.962038
1	-4.190118	0.871296	-13.592026	0.872248	-29.561631	0.961647
2	-2.825671	0.870241	-12.140217	0.871008	-28.057974	0.960864
3	-1.565859	0.868659	-10.748196	0.869137	-26.587937	0.959687
4	-0.412507	0.866556	-9.416321	0.866620	-25.151583	0.958112
5	0.631818	0.863940	-8.145078	0.863435	-23.748993	0.956134
6	1.563669	0.860831	-6.935088	0.859556	-22.380270	0.953747
7	2.378513	0.857268	-5.787122	0.854948	-21.045541	0.950943
8	3.070409	0.853324	-4.702111	0.849568	-19.744953	0.947712
9	3.631486	0.849126	-3.681163	0.843360	-18.478676	0.944045
10	4.051055	0.844797	-2.725589	0.836258	-17.246904	0.939928
20	0.291969	0.002625	2.706651	0.672645	-6.888698	0.869535
30	0.037042	0.000053	0.641135	0.020307	-0.419007	0.713687
40	0.008906	0.000004	0.144416	0.001099	1.517671	0.342971
50	0.002950	0.000001	0.047344	0.000143	0.735440	0.046208
60	0.001195	0.000000	0.019124	0.000028	0.304559	0.007705
70	0.000557	0.000000	0.008891	0.000007	0.142053	0.001837
80	0.000288	0.000000	0.004579	0.000002	0.073205	0.000545
90	0.000161	0.000000	0.002550	0.000001	0.040765	0.000188
100	0.000097	0.000000	0.001510	0.000000	0.024137	0.000073

Note. For complex optical LJ(12, 6) potential with $B = C = 125$, $s = 10$, at three values of reduced energy K.

phase shifts for these systems have been reported before [10, 18], the accuracy of the results of Table III which is needed for these strongly absorptive potentials is hardly obtainable by other methods using the real line as the integration path. With the present method, due to the correct complex integration path, phase shifts of virtually any desired accuracy can be computed routinely for almost any complex potential.

8. Conclusions

A computation procedure for fully complex Prüfer phase function calculations has been described and applied to several computationally different problems. Apart from the complex Sturm–Liouville eigenvalue problem, applications in which the desired quantity is related to the value of the phase function or to another function obtained by partial differentiation of the phase function with respect to one of the parameters or to a complicated system of such functions have been considered. The heart of the method is the analysis of the relevant integration paths which enable the integrations to be performed by the computationally efficient phase integral quadrature and modified Prüfer phase function integration procedures. The present illustrations deal with scattering theory but it is clear that many other problems in applied mathematics, physics, chemistry, and engineering would have a natural formulation as a complex Prüfer phase function calculation.

References

1. H. Prüfer, *Math. Ann.* **95**, 499 (1926).
2. P. B. Bailey, *SIAM J. Appl. Math.* **14**, 242 (1966).
3. B. A. Hargrave, *J. Comput. Phys.* **20**, 381 (1976).
4. P. B. Bailey, *J. Comput. Phys.* **29**, 306 (1978).
5. P. Pajunen and J. Tienari, *J. Comput. Phys.* **65**, 159 (1986).
6. P. Pajunen, *J. Molec. Spectrosc.* **124**, 185 (1987).
7. P. B. Bailey, M. K. Gordon, and L. F. Shampine, *ACM Trans. Math. Software* **4**, 193 (1978).
8. *Numerical Algorithms Group, Fortran Library*, Routine Documents D02KAF, D02KDF, D02KEF, Mark 11 (1984) (unpublished).
9. P. Pajunen and J. Luppi, *J. Chem. Phys.* **82**, 5118 (1985).
10. B. C. Eu, *J. Chem. Phys.* **52**, 3021 (1970).
11. J. Luppi and P. Pajunen, *J. Chem. Phys.* **81**, 1836 (1984).
12. P. Pajunen and R. J. Le Roy, *J. Chem. Phys.* **77**, 3527 (1982).
13. J. Luppi and P. Pajunen, *J. Chem. Phys.* **78**, 4451 (1983).
14. K. Ford and J. Wheeler, *Ann. Phys. (NY)* **7**, 259 (1959).
15. M. S. Child, *Molecular Collision Theory* (Academic Press, London, 1974), Chap. 5.
16. J. N. L. Connor, *Semiclassical Methods in Molecular Scattering and Spectroscopy*, edited by M. S. Child (Reidel, Dordrecht, 1980), Chap. 2, p. 45.
17. E. A. Remler, *Phys. Rev. A* **3**, 1949 (1971).
18. J. N. L. Connor, D. C. Mackay, and K.-E. Thylwe, *J. Chem. Phys.* **85**, 6368 (1986).